Low-energy elastic electron scattering from isobutanol and related alkyl amines

Kamil Fedus, C. Navarro, L. R. Hargreaves, M. A. Khakoo, F. M. Silva, M. H. F. Bettega, C. Winstead, and V. McKoy

Phys. Rev. A **90**, 032708 — Published 8 September 2014

DOI: 10.1103/PhysRevA.90.032708

LOW-ENERGY ELASTIC ELECTRON SCATTERING FROM ISOBUTANOL AND RELATED ALKYL AMINES

Kamil Fedus

Institute of Physics, Faculty of Physics, Astronomy and Informatics, Nicolaus Copernicus University, Grudziadzka 5, 87-100 Torun, Poland, EU,

C. Navarro, L. R. Hargreaves and M. A. Khakoo

Department of Physics, California State University, Fullerton, CA 92831, USA,

F. M. Silva and M. H. F. Bettega,

Departamento de Física, Universidade Federal do Paraná, Caixa Postal 19044, 81531-990 Curitiba, Paraná, Brazil

and

C. Winstead and V. McKoy.

A. A. Noyes Laboratory of Chemical Physics, California Institute of Technology, Pasadena, California 91125, USA.

ABSTRACT: Normalized experimental differential and integral cross sections for vibrationally elastic scattering of low-energy electrons from isobutanol (C_4H_9OH) are presented. The differential cross sections are measured at incident energies from 1 to 100 eV and scattering angles from 5^o to 130^o. These cross sections are compared to earlier experimental and theoretical results for isobutanol and *n*-butanol, as well as to results for smaller alcohols and for alkanes. Further comparisons are made with calculated cross sections for isobutylamine ($C_4H_9NH_2$) and for smaller amines including ethylamine ($C_2H_5NH_2$), dimethylamine ($CH_3NH_2CH_3$), the two $C_3H_9NH_2$ isomers *n*-propylamine and isopropylamine, and ethylene diamine ($NH_2C_2H_2NH_2$). The calculated

cross sections are obtained using the Schwinger multichannel method. The comparisons illuminate the role of molecular structure in determining the angular distribution of resonantly scattered electrons.

PACS number(s): 34.80.Bm, 34.80.Gs

1. Introduction

Low-energy electron collisions with gaseous molecules containing a hydroxyl (OH) group have provided useful information regarding the collision physics involving molecules with a permanent dipole moment. Differential cross sections (DCSs) for these species have been measured for targets including water [1] and primary alcohols [2,3]. Recently Bettega et al. investigated low-energy electron scattering from four butanol (C_4H_9OH) isomers (*n*-, iso-, 2- and *t*-butanol) using the Schwinger multichannel method within the static-exchange plus polarization approximation [4], and found that different partial-wave contributions to the resonant DCS behavior of these isomers (*d*-wave or *f*-wave oscillatory pattern) depended on their structure (branched or straight-chain). Their investigation expanded on earlier work that showed a similar pattern in electron scattering by smaller alcohols [2,3] and by straight- and branched-chain alkanes. Studies of OH-containing molecules are also of interest in light of recent work by Allan and co-workers on dissociative electron attachment (DEA) to various alcohols [5] that indicated the presence of an H σ* resonance whose influence increased with the size of the molecule, while similar studies [6] of asymmetric ethers revealed pronounced energy selectivity in which C–O bond is broken, as well as a general tendency against breaking O–CH_3 bonds. Such DEA results provide important information about where on the molecule the impinging electron attaches to form a resonance (temporary anion) and about which molecular features—for example, the size, the presence or absence of substituent groups, and the arrangement of atoms—are most significant in determining the electron scattering behavior and subsequent nuclear dynamics. This information is of great interest at present because it appertains to low energy electron-driven damage to biological molecules such as DNA, which predominantly involves DEA processes [7]. The present experimental work was primarily undertaken to provide data for comparison with our earlier

results on low energy elastic electron scattering from *n*-butanol [3] and to explore the observation in theoretical work [4], mentioned above, that isobutanol exhibits a *d*-wave scattering pattern in the DCS, vs. an *f*-wave pattern in *n*-butanol, in the resonant region near 10 eV collision energy.

In addition to the measurements on isobutanol, we have also performed calculations using the Schwinger multichannel method for electron scattering from $C_4H_9NH_2$ (isobutylamine), where the hydroxyl (OH) group has been replaced by an isoelectronic amide (NH_2) group (see Fig. 1), and on five smaller alkyl amines, ethylamine, dimethylamine, *n*-propylamine, isopropylamine, and ethylene diamine (Fig. 2), in order to explore whether the patterns observed in the DCS persist when OH is replaced with NH_2. We note that the dipole moments of the butyl alcohols are similar, ranging around 1.69 to 1.81 D, and that of isobutylamine is 1.1 to 1.3 D [9].

2.1. Experimental

Our experimental apparatus (spectrometer, vacuum chamber, control equipment) has been detailed in previous papers, e.g. Khakoo et al. [10], and a brief description will be given here. Both the electron gun and detector employed double hemispherical energy selectors, and the apparatus was made of titanium. Cylindrical lenses were used to transport scattered electrons through the system which was baked to about 130^o with magnetically free biaxial heaters [11]. Electrons were detected by a discrete dynode electron multiplier [12] with a dark count rate of <0.01Hz and capable of linearly detecting $>10^5$ Hz without saturating. The remnant magnetic field in the collision region area was reduced to ≈1mG at the collision region by a double μ-metal shield, coupled with a Helmholtz coil that eliminated the vertical component of the Earth's magnetic field. Typical electron currents were around 18-28 nA, with an energy resolution of between 40-50meV, full-width at half-maximum. Lower currents were chosen for lower E_0 values in order to curtail the

effects of space charge broadening of the incident electron beam. The electron beam could be easily focused at 1 eV and remained stable, varying less than 15% at maximum during the day's data acquisition. The energy of the beam was established by repetitively (at least daily) measuring the dip in the elastic scattering of the 2^2S He- resonance at 19.366eV [13] at $\theta=90^o$ to better than ≈30meV stability during an experimental run (1 day). Typically the contact potential varied from 0.6 eV to 0.7 eV. Energy loss spectra of the elastic peak were collected at fixed E_0 values and θ by repetitive, multi-channel-scaling techniques. The effusive target gas beam was formed by flowing gas through a 0.3mm diameter aperture, which was sooted (using an acetylene flame) to reduce secondary electrons. In using the aperture instead of a conventional tube gas collimator, we obviate the experimental need to maintain the gas pressures of the target gases in an inverse ratio of their molecular diameters, thus removing an additional systematic source of error that could occur in using tube collimators or similar, see e.g. [3]. The aperture, located ≈5-7mm below the axis of the electron beam, was incorporated into a moveable source [14] arrangement. The moveable gas source method determines background electron-gas scattering rates expediently and accurately [15]. The measured DCSs were normalized using the Relative Flow Method with helium as the reference gas, using DCSs from the well-established work of Nesbet [15] for E_0 below 20eV and of Register et al. [16] for E_0 above 20eV. The pressures behind the aperture ranged from 1.2 to 2 torr for He and 0.08 to 0.14 torr for isobutanol, resulting in a chamber pressure ranging from $1.2x10^{-6}$ torr to $2x10^{-6}$ torr. Each DCS was taken a minimum of two times to check its reproducibility and weighted averaging was made of multiple data sets to obtain the final DCSs.

2.1.1. DCS Integration

Integral cross sections (ICS) and Momentum Transfer Cross Sections (MTCS) were evaluated from the measured DCS by extrapolating the DCS to zero and 180 degrees and applying the

standard integral formula. Per several previous studies reported by this group [1-3], the Born-Dipole DCS was used to estimate the contribution to the ICS from small scattering angles, which for polar targets is expected to be much larger (as much as 5 orders of magnitude) than a simple extrapolation from the measured data would indicate. A dipole moment of 1.66 D was assumed [17], while 5 meV of inelasticity was included to prevent a non-integrable singularity that occurs at 0 degrees for a completely elastic transition.

In this study, we employed a different extrapolation method from the one we have used in the past, which eliminates some numerical convergence issues encountered previously while trying to implement a Born-Dipole guided extrapolation routine. The routine is first described excluding incorporation of the Born Dipole cross section. Each DCS was extrapolated to zero degrees by fitting a cubic polynomial to the measured data points for the three smallest angles. Three data points do not specify a unique 3^{rd} order polynomial, allowing the additional condition that the polynomial's first derivative must equal zero at zero degrees. Once the polynomial coefficients are found, the value of the DCS was simply evaluated from the polynomial at zero degrees. This extrapolation routine was then repeated using the 3 data points for the largest angles to estimate the DCS at 180 degrees. Once both endpoint values are obtained, the entire DCS was interpolated with a standard cubic spline fit and integrated.

The above procedure is a very simple method of estimating the values of the DCS at the endpoints, but nonetheless always yielded a smooth DCS (free from spurious structures) with visually plausible endpoints, whilst avoiding the subjectivity of a 'by-eye' extrapolation. This routine is also simple to modify to account for the forward angle scattering. First, the value of the Born Dipole DCS was subtracted from the measured DCS at each measured angle. The ICS for this subtracted DCS was then determined according to the above procedure. Since the Born DCS

has been subtracted, we refer to this ICS as the "non-dipole" ICS, which we interpret as an estimate of the contribution to the DCS arising from scattering processes other than the long range dipole scattering.

The dipole contribution to the ICS was determined by evaluating the analytic form of the ICS in the Born approximation for scattering from a point dipole, given as:

$$ICS_{Born} = \frac{4}{3}\pi\mu^2 \frac{\ln[(k_i + k_f)^2] - \ln[(k_i - k_f)^2]}{k_i^2} \qquad (1),$$

where k_i and k_f are the incident and scattered electron momenta respectively, and μ is the dipole moment (all in atomic units). The sum of the "dipole" and "non-dipole" contributions to the ICS gives the final value of the ICS.

2.2. Theoretical

The cross sections for electron collisions with isobutylamine were computed with the Schwinger multichannel (SMC) method. The SMC method and its implementation with pseudopotentials (SMCPP), which was used in the present calculations, were described in detail elsewhere [18,19]. Therefore, we will only discuss the theoretical aspects related to the present calculations.

The ground state geometry of isobutylamine was optimized at the level of second order Möller-Plesset perturbation theory within the C_1 group using the 6-311++(2d,1p) basis set with the package GAMESS [20]. The calculated value for the dipole moment is 1.26 D. In the scattering calculations we employed the pseudopotentials of Bachelet, Hamann and Schlüter [21] to replace the core electrons of the carbon and the nitrogen atoms. We used a basis set with five *s*-type, five *p*-type, and two *d*-type functions [22] generated according to [23]. For the hydrogens we used the 4s/3s basis set of Dunning [24] augmented with one *p*-type function with exponent 0.75. To describe the polarization effects we used improved virtual orbitals (IVOs) [25] to represent the

hole and the particle orbitals. We considered single virtual excitations of the target, considering both singlet- and triplet-coupled excitations, from the 16 occupied orbitals to the lowest 26 IVOs, giving the total of 11011 configuration state functions in the expansion of the scattering wave function. We employed the standard Born-closure procedure [26] to account for scattering of the higher partial waves due to the long-range character of the dipole potential.

Elastic electron scattering cross sections for ethylamine, dimethylamine, *n*-proplyamine, isopropylamine, and ethylenediamine were carried out using an all-electron version of the SMC method implemented for massively parallel computers [27]. The geometry for each molecule was optimized at the level of second-order Möller-Plesset perturbation theory within the 6-31G(*d*) Gaussian basis set as contained in GAMESS [20], subject to symmetry constraints that required a C_s conformation for the first three molecules and a C_{2h} conformation for butylenediamine. For the scattering calculation, the same one-electron basis set was used in each case, namely the double-zeta valence basis of Dunning [28] supplemented, on the heavy atoms, by two *d*-type polarization functions plus one diffuse *s* and one diffuse *p* function, and on the hydrogens by a *p* polarization and *s* diffuse function. Default exponents and splitting factors as contained in GAMESS [20] were used for the supplementary functions. The molecular ground state was described by a restricted Hartree-Fock wave function. An orthogonal transformation was applied to the Hartree-Fock virtual molecular orbitals to obtain the modified virtual orbitals of Bauschlicher [29], in each case using a +6 cation Fock operator. To describe polarization effects, the many-electron variational basis set for the SMC scattering calculations included doublet configuration state functions formed from singlet-coupled single excitations from the valence orbitals of the target molecule into the 30 lowest-energy modified virtual orbitals. The total size of the variational space was 25148 configuration state functions for each of ethylamine and dimethylamine, 44784

for each of *n*-propylamine and isopropylamine, and 42438 for ethylenediamine. The differential cross sections were corrected for long-range scattering by the dipolar potential using the approach previously described [30], except in the case of ethylene diamine, which is nonpolar in the C_{2h} conformation.

3. Results and Discussion.

We measured normalized experimental elastic scattering DCSs for electron scattering from isobutanol for E_0 values from 1 to 100 eV and θ from 5° to 130°. These DCSs are listed in Table 1 along with 1 standard deviation errors determined from the statistical counts, reproducibility of the DCSs, and estimated errors in gas flow-rates (2% for each gas) and in the helium elastic DCSs (5 to 7%).

Figure 3 compares the present experimental DCSs at selected E_0 values with our present SMC calculations for isobutylamine, our previous calculations for isobutanol [4], and our previous measurements and calculations for *n*-butanol [3]. At E_0=1 eV to 15 eV the experimental DCSs of isobutanol and *n*-butanol are similar in magnitude and, to some extent, shape. At higher energies the agreement between the measured isobutanol and n-butanol DCSs improves, and at 30eV and above (note that 50 and 100eV results are not shown) they become essentially identical. At 1eV both follow the shape of the Born-dipole curve at small θ but are about 20-40% larger. At 1 eV, the calculated DCSs agree well with experiment at forward angles but do not show the backward peaking seen in the measurements; however, at 2 to 10 eV, there is good qualitative and semi-quantitative agreement between calculation and experiment. At $E_0 \geq 10$ eV, the qualitative agreement continues to be good, although from 20 eV and up the calculations produce DCSs that are too large at intermediate angles, as is typical of single-channel calculations that neglect loss of

flux into excitation and ionization channels. Note that the SMC results for isobutylamine are highly similar to those for isobutanol at all energies.

Figure 4a shows the so-called excitation function at 90^o, that is, the DCS measured as a function of E_0 at a fixed scattering angle. This displays a broad peak, probably due to one or more shape resonances, between 5 and 15eV, with a maximum at approximately 8.5 eV, after taking qualitatively into account the direct-scattering background. We observed similar broad resonances in other alcohols [2-4, 31] and noted that they show qualitatively different behavior of the DCS depending on whether the molecule has a straight- or branched-chain structure. To investigate this resonant behavior, we have taken detailed DCS measurements at 10 eV on both isobutanol and *n*-butanol and normalized our present relative *n*-butanol DCSs to our earlier DCSs [3] for *n*-butanol. Our results (Fig. 4b) show clear differences in the DCSs between isobutanol and *n*-butanol at 10 eV, as predicted by theory. Whereas *n*-butanol shows a minimum around 90^o, reflective of the *f*-wave pattern typically seen in straight-chain molecules such as ethanol [2] and *n*-propanol [3], isobutanol shows instead a "*d*-wave" shape, with a peak at 90^o, consistent with the pattern seen in resonant scattering by other branched systems such as isopropanol [31]. Although the oscillations in the measurements are less pronounced than predicted by theory, the experiment can clearly differentiate between the two targets. We note that the calculated DCS for isobutylamine at 10 eV (Fig. 3) likewise shows the *d*-wave pattern, with a local maximum at 90^o.

Further information on the connection between resonant scattering patterns and molecular structure comes from a consideration of other alkyl amines. In a recent study, Silva et al. [32] computed elastic electron and positron scattering cross sections for methylamine, CH_3NH_2. Their electron DCS at 10 eV shows the *f*-wave pattern expected for unbranched-chain molecules. In Fig. 5, we show our present calculated results at 10 eV for five additional amines, four of which have a

straight-chain structure while one, isopropylamine, has a branched structure (see Fig. 2). These molecules fit the overall trend with the exception of dimethylamine, which shows a (mostly) *d*-wave pattern despite having a straight-chain structure. We note that other exceptions exist; for example, the simplest alcohol, methanol, does not show an *f*-wave pattern. Nonetheless, the overall trend is strong, and recent calculations on the five-carbon straight-chain alcohol *n*-pentanol [33] show that it extends to even larger systems as well as to other amines [34].

Figure 6 shows integral elastic cross sections (ICS) and momentum transfer cross sections (MTCS) for isobutanol and *n*-butanol. The ICS and MTCS values plotted for *n*-butanol differ slightly from those reported in [3] and are obtained by applying the extrapolation routine described above to the DCS data given in [3], for consistency of comparison. Our Born-corrected experimental ICS data are in very good agreement with the results of the SMC calculations (which also include a Born-dipole correction). The poorer agreement with theory when the Born correction is not applied shows the importance of the dipole interaction at small collision energies E_0, while at $E_0 \geq 15$eV, the two differently extrapolated ICSs merge as expected due to the lessening influence of dipolar scattering. Because the contribution of the DCS to the momentum transfer cross section goes to zero at small angles, the Born-dipole extrapolation and the polynomial extrapolation give the same MTCSs, so we have only provided one MTCS for each target. Here we see good overall agreement with the calculations for both molecules. We note the relatively sharp resonance, seen by theory at E_0=10eV, is observed in both the ICSs and MTCS measurements.

The present calculated results for isobutylamine, obtained using the extrapolation process described in Sec. 2.1.1 with an assumed inelasticity of 5 meV, are also shown in Fig. 6. At small E_0, both the MTCS and, especially, the ICS of isobutylamine are somewhat smaller than those of

isobutanol, as would be expected due to isobutylamine's smaller dipole moment, but the cross sections for the two molecules agree closely above roughly 5 eV.

4. Conclusions.

We have presented experimental DCSs for elastic electron scattering from isobutanol obtained using an aperture, moveable gas beam source interfaced with an electron spectrometer in an effort to investigate similarities and differences among the butyl alcohols seen in calculations [4]. The experimental results confirm an overall similarity in magnitude between the DCSs for isobutanol and *n*-butanol, especially at high energies. Our measurements also verify the prediction [4] that the DCS of isobutanol shows a dominant *d*-wave symmetry in the resonant region near 10 eV, in contrast to the *f*-wave symmetry seen in *n*-butanol. The present calculations for the isoelectronic molecule isobutylamine produce cross sections highly similar to those of isobutanol, including the *d*-wave scattering pattern, while results for five smaller alkyl amines support the general trend of branched molecules showing a *d*-wave pattern and unbranched molecules an *f*-wave pattern.

The underlying reasons for this trend are not fully clear. Shape-resonant scattering can often be usefully analyzed in terms of the energies and symmetries of the lowest unoccupied valence orbitals. In the alkanes, alkyl alcohols, and alkyl amines, these are mostly C-C, C-O, and/or C-N σ^* orbitals. Thus in ethane (C_2H_6), where the lowest-energy empty valence orbital is C-C σ^* and has an obvious f_{z^3} shape, it is not surprising to find that the resonant DCS exhibits a pattern characteristic of *f*-wave scattering. However, it is less obvious what controls the scattering pattern in larger alkanes with multiple C-C σ^* resonances, and in particular what differentiates branched from unbranched systems. Similar remarks apply to the alcohols and amines. It is perhaps suggestive that two exceptions to the *f*-wave trend among unbranched molecules, methanol and

dimethylamine, lack C-C bonds; however, methylamine, which also lacks a C-C bond, does exhibit an *f*-wave DCS at 10 eV [32]. Despite these open questions, that the same trend should persist (with limited exceptions) across a broad family of molecules (alkanes, alkyl alcohols, alkyl amines) despite wide differences in size, dipole moment, etc., is itself remarkable.

5. Acknowledgements.

K. F. acknowledges the Fulbright Program for a fellowship to conduct this work at California State University Fullerton. M. A. K. and L. R. H. acknowledge support from National Science Foundation research grants NSF-RUI-AMO 1306742 and 0968874. F.M.S. acknowledges support from Brazilian Agency Coordenação de Aperfeiçoamento de Pessoal de Nível Superior (CAPES). M.H.F.B. acknowledges support from Brazilian agencies Conselho Nacional de Desenvolvimento Científico e Tecnológico (CNPq), and FINEP (under project CTInfra). F.M.S and M.H.F.B also acknowledge computational support from Professor Carlos M. de Carvalho at LFTC-DFis-UFPR and at LCPAD-UFPR, and from CENAPAD-SP. The work of V.M. and C.W. was supported by the Chemical Sciences, Geosciences and Biosciences Divsion, Office of Basic Energy Sciences, Office of Science, U.S. Department of Energy under Grant DE-FG02-97ER14814 and made use of the Jet Propulsion Laboratory's Supercomputing and Visualization Facility.

6. References.

[1] M. A. Khakoo, H. Silva, J. Muse, M. C. A. Lopes, C. Winstead, and V. McKoy, Phys. Rev. A **78**, 052710 (2008); erratum, Phys. Rev. A **87,** 049902 (2013).

[2] M.A. Khakoo, J. Blumer, K. Keane, C. Campbell, H. Silva, M.C.A. Lopes, C. Winstead, V. McKoy, R.F. da Costa, L.G. Ferreira, M.A.P. Lima, and M.H.F. Bettega, Phys. Rev. A **77**, 042705 (2008).

[3] M.A. Khakoo, J. Muse, H. Silva, M.C.A. Lopes, C. Winstead, V. McKoy, E.M. de Oliveira, R.F. da Costa, M.T. do N. Varella, M.H.F. Bettega, and M.A.P. Lima, Phys. Rev. A **78**, 062714 (2008).

[4] M. H. F. Bettega , C. Winstead and V. McKoy, Phys. Rev. A **82,** 062709 (2010).

[5] B. C. Ibănescu, O. May, A. Monney and M. Allan, Phys. Chem. Chem. Phys. **9,** 3136 (2007).

[6] B. C. Ibănescu and M. Allan, Phys. Chem. Chem. Phys. **9** 3136 (2009).

[7] L. Sanche, Eur. Phys. J. D **35**, 367 (2005).

[8] L. Caron, L. Sanche, S. Tonzani and C. Greene, Phys. Rev. A **80,** 012705 (2009).

[9] NIST Computational Chemistry Comparison and Benchmark Database, NIST Standard Reference Database Number 101, Release 16a, August 2013, Russell D. Johnson III, editor. http://cccbdb.nist.gov/

[10] M. A. Khakoo, C. E. Beckmann, S. Trajmar and G. Csanak, Phys. Rev. A **27**, 3159 (1994).

[11] ARi Industries Inc., Addison, IL 60101 USA, 1HN040B-16.3 biaxial cable.

[12] ETP Equipe Thermodynamique et Plasmas (ETP) model AF151.

[13] J. H. Brunt, G. C. King, and F. H. Read, J. Phys. B: At. Mol. Phys. **10**, 1289 (1977).

[14] M. Hughes, K. E. James, Jr., J. G. Childers, and M. A. Khakoo, Meas. Sci. Technol. **14**, 841 (1994).

[15] R. K. Nesbet, Phys. Rev. A **20**, 58 (1979).

[16] D. F. Register, S.Trajmar, and S. K. Srivastava, Phys. Rev. A **21**, 1134 (1980).

[17] CRC Handbook of Chemistry and Physics, 64th Edition (1983-4), CRC Press, Inc., Editor: R. C. Weast, Boca Raton, Florida, USA.[18] K. Takatsuka and V. McKoy, Phys. Rev. A **24**, 2473 (1981); **30**, 1734 (1984).

[19] M. H. F. Bettega, L. G. Ferreira, and M. A. P. Lima, Phys. Rev. A **47**, 1111 (1993).

[20] M.W. Schmidt, K. K. Baldridge, J. A. Boatz, S. T. Elbert, M. S. Gordon, J. H. Jensen, S. Koseki, N. Matsunaga, K. A. Nguyen, S. J. Su, T. L. Windus, M. Dupuis, and J. A. Montgomery, J. Comput. Chem. **14**, 1347 (1993).

[21] G. B. Bachelet, D. R. Hamann, and M. Schl¨uter, Phys. Rev. B **26**, 4199 (1982).

[22] F. Kossoski and M. H. F. Bettega, J. Chem. Phys. **138**, 234311 (2013).

[23] M. H. F. Bettega, A. P. P. Natalense, M. A. P. Lima, and L. G. Ferreira, Int. J. Quantum Chem. **60**, 821 (1996).

[24] T. H. Dunning, Jr., J. Chem. Phys. **53**, 2823 (1970).

[25] W. J. Hunt and W. A. Goddard, III, Chem. Phys. Lett. **3**, 414 (1969).

[26] E. M. de Oliveira, R. F. da Costa, S. d'A. Sanchez, A. P. P. Natalense, M. H. F. Bettega, M. A. P. Lima, and M. T. do N. Varella, Phys. Chem. Chem. Phys. **15**, 1682 (2013).

[27] C. Winstead and V. McKoy, Comput. Phys. Commun. **128**, 386 (2000).

[28] T. H. Dunning, Jr., and P. J. Hay, in *Methods of Electronic Structure Theory,* H. F. Schaefer III, editor (Plenum, New York, 1977), p. 1.

[29] C. W. Bauschlicher, Jr., J. Chem. Phys. **72**, 880 (1980).

[30] T. N. Rescigno and B. H. Lengsfield III, Phys. Rev. A **45**, 2894 (1992), and references therein.

[31] M. H. F. Bettega, C. Winstead, V. McKoy, A. Jo, A. Gauf, J. Tanner, L. R. Hargreaves, and M. A. Khakoo, Phys Rev. A **84**, 042702 (2011).

[32] F. M. Silva, M. H. F. Bettega, and S. d'A. Sanchez, Eur. Phys. J. D **68**, 12 (2014).

[33] E. M. de Oliveira, M. T. do N. Varella, M. H. F. Bettega and M. A. P. Lima, Eur. Phys. J. D **68**, 65 (2014).

[34] F. M. Silva, M.Sc. Thesis, Universidade Federal do Paraná, Curitiba, Paraná, Brazil (2013).

Angle (°)	ieV	Error	2eV	Error	3eV	Error	5eV	Error	10eV	Error	15eV	Error	20eV	Error	30eV	Error	50eV	Error	100eV	Error
5																	107.7	9.0	127.1	11.5
10											34.3	3.1	63.1	5.4	53.6	4.5	61.8	4.9	33.5	3.2
15											26.2	2.2	36.6	4.2	28.3	2.2	22.6	1.7	6.73	0.57
20			12.5	0.6			18.0	2.2	16.6	1.5	16.2	1.5	19.0	1.8	11.5	1.0	6.72	0.52	3.15	0.29
25	16.9	1.6	7.96	0.63	7.35	0.66	10.37	1.27	10.68	0.93	9.28	0.75	8.97	0.85	4.89	0.38	3.09	0.24	2.19	0.21
30	12.0	1.2	5.27	0.39	6.20	0.51	7.09	0.67	6.92	0.57	5.74	0.48	4.59	0.41	3.35	0.27	2.43	0.19	1.34	0.13
40	5.01	0.55	3.05	0.23	3.75	0.33	4.00	0.34	3.36	0.27	3.75	0.32	3.23	0.26	2.40	0.20	1.43	0.13	0.657	0.067
50	2.97	0.27	2.87	0.23	3.26	0.27	3.53	0.29	3.01	0.24	3.29	0.27	2.80	0.22	1.63	0.13	0.861	0.072	0.390	0.035
60	2.55	0.36	2.85	0.22	3.41	0.28	3.38	0.36	2.51	0.23	2.40	0.20	1.89	0.15	1.12	0.11	0.537	0.054	0.310	0.051
70	2.29	0.23	2.74	0.22	2.93	0.24	2.65	0.21	2.14	0.17	1.90	0.16	1.41	0.11	0.780	0.064	0.369	0.037	0.163	0.018
80	2.23	0.21	2.46	0.21	2.57	0.21	2.20	0.17	1.95	0.15	1.63	0.15	1.11	0.09	0.570	0.057	0.296	0.029	0.106	0.017
90	2.92	0.27	2.14	0.22	2.11	0.17	2.22	0.18	2.06	0.16	1.44	0.12	0.97	0.08	0.507	0.044	0.231	0.019	0.132	0.014
100	2.72	0.27	1.76	0.14	1.70	0.14	2.16	0.18	1.99	0.18	1.44	0.15	0.97	0.08	0.517	0.047	0.245	0.021	0.141	0.044
110			1.42	0.12	1.59	0.12	2.35	0.18	1.89	0.16	1.52	0.15	1.06	0.09	0.597	0.046	0.266	0.025	0.189	0.023
120			1.19	0.10	1.59	0.13	2.12	0.18	1.79	0.15	1.52	0.12	1.13	0.09	0.743	0.064	0.353	0.038	0.185	0.021
125					1.575	0.129														
130							2.28	0.18	2.09	0.16	1.77	0.14	1.39	0.11	0.929	0.078	0.463	0.039	0.210	0.023
ICS_{corr}	116.16	13.3	69.33	3.04	60.38	2.44	65.99	7.33	52.96	6.14	46.27	3.94	46.24	4.36	32.21	2.82	25.41	1.78	16.51	2.41
ICS_{uncorr}	57.57	13.3	34.52	3.04	34.22	2.44	49.47	7.33	43.72	6.14	40.31	3.94	41.75	4.36	28.91	2.82	23.48	1.78	15.45	2.41
MTCS	23.87	2.96	20.43	1.81	24.06	1.84	33.75	4.16	31.09	4.81	25.52	3.69	19.90	3.11	11.99	1.54	6.21	0.90	3.00	0.51

Table 1: Present experimental DCSs, ICSs and MTCSs for elastic scattering of electrons from isobutanol. Units for DCS are in 10^{-16}cm^2/sr and for ICSs and MTCSs are in 10^{-16}cm^2, respectively. See text for discussion.

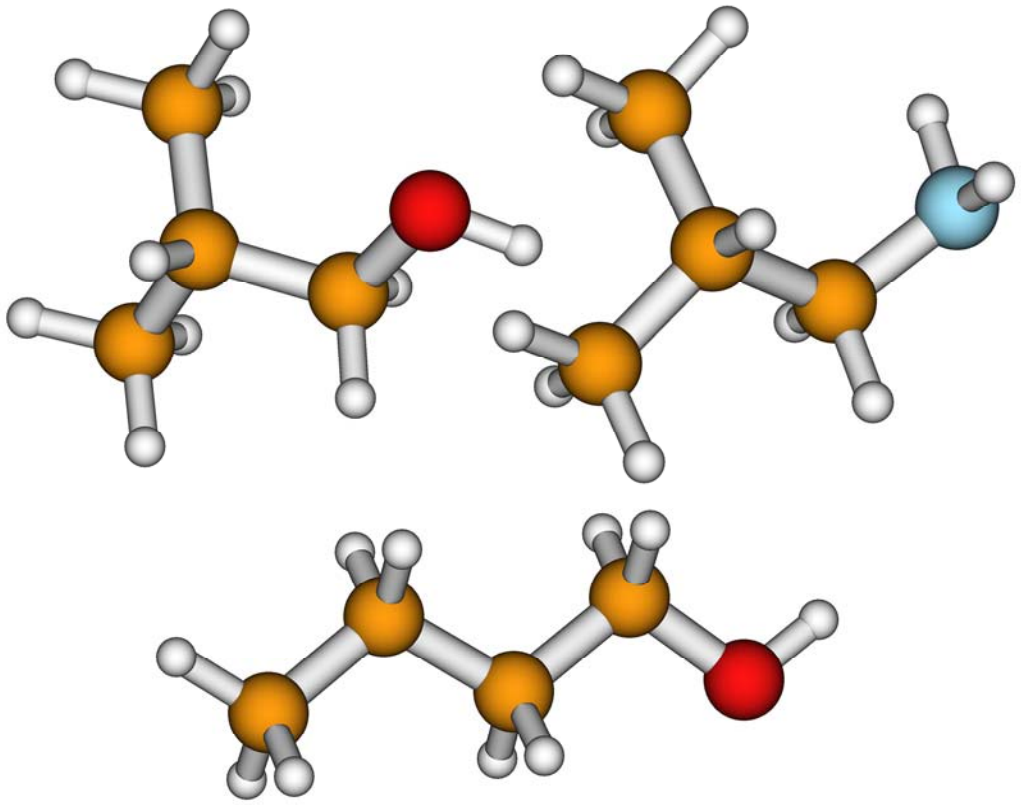

Figure 1 (color online). Ball and stick models of the structures of isobutanol (upper left), isobutylamine (upper right), and *n*-butanol (bottom). Small white spheres are hydrogen atoms, dark spheres are carbons (brown) or oxygen (red), and the light blue sphere is nitrogen.

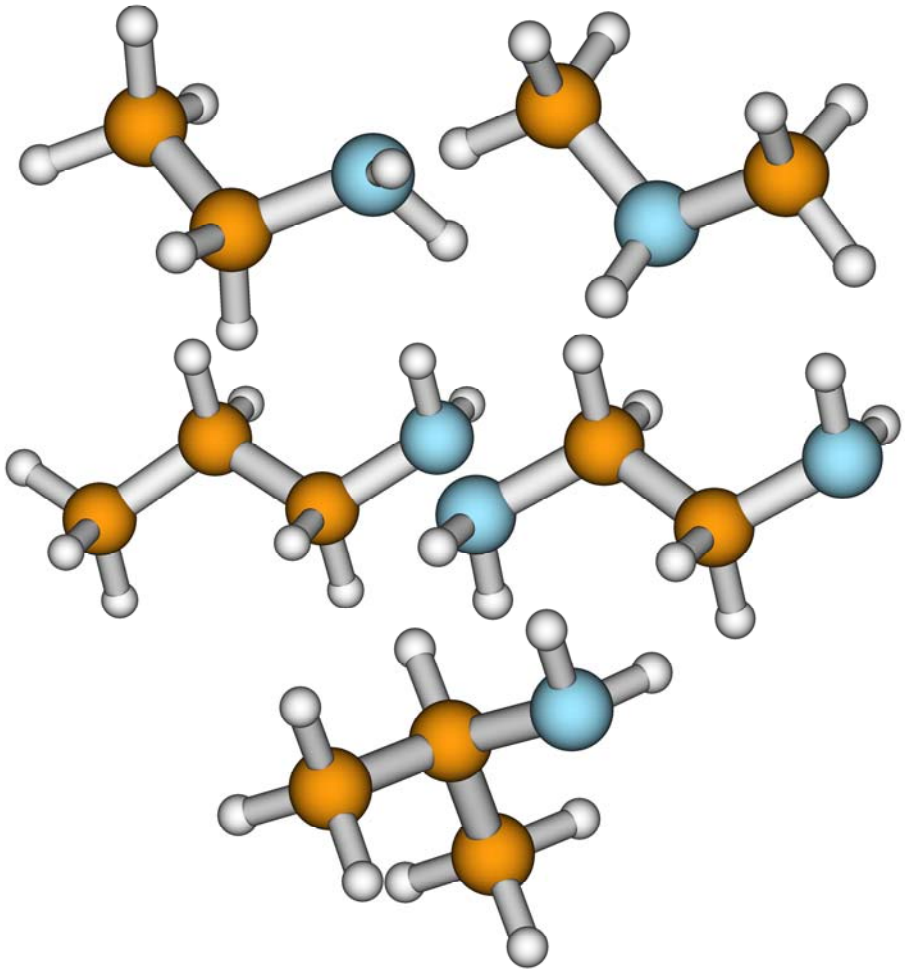

Figure 2 (color online). Structures of small alkyl amines studied in the present work: ethylamine (upper left), dimethylamine (upper right), *n*-propylamine (center left), ethylene diamine (center right), and isopropylamine (bottom). Small white spheres are hydrogen atoms, dark brown spheres are carbons, and light blue spheres are nitrogens.

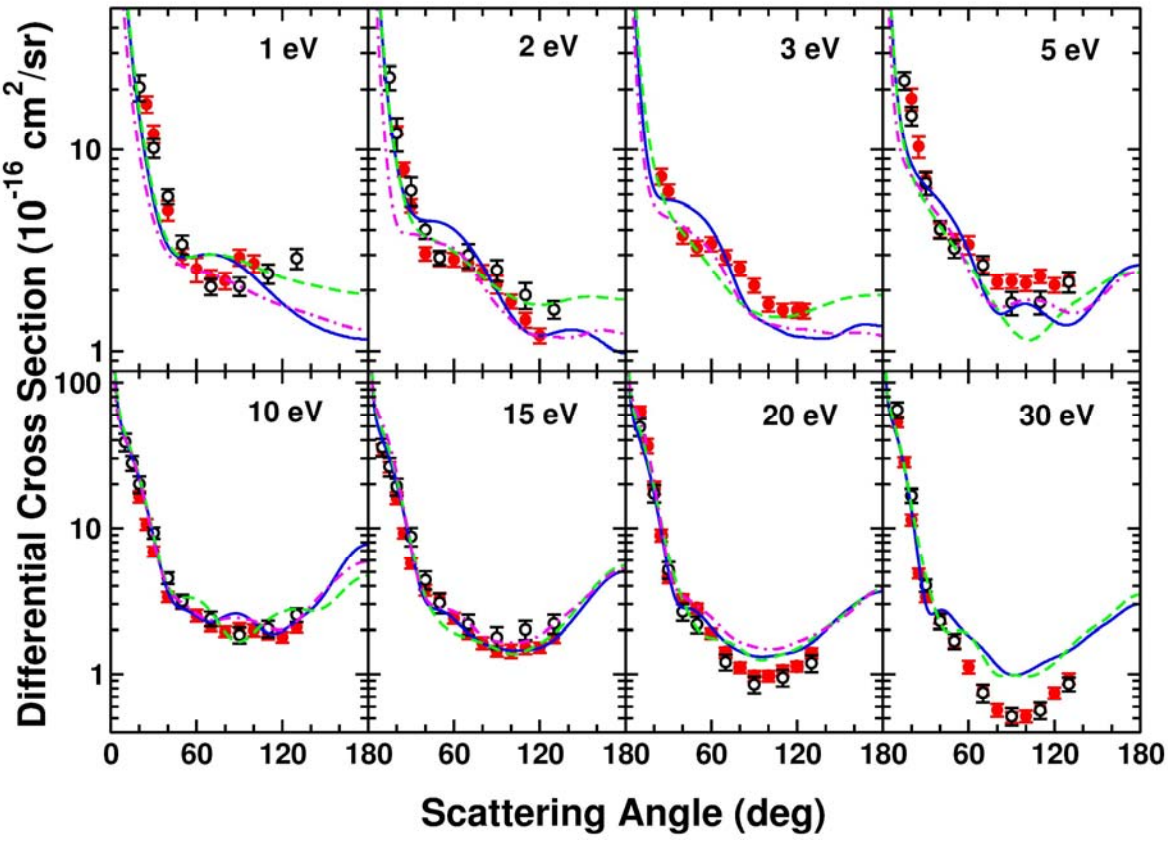

Figure 3 (color online)**.** Comparison of present measured DCSs for elastic electron scattering by isobutanol with earlier results. Filled red circles are present isobutanol measurements; open circles are *n*-butanol measurements of Ref. 8; solid blue line is the isobutanol calculation of Ref. 4; dashed green line is the pseudopotential calculation for *n*-butanol of Ref. 8; and chained magenta line is the present calculated result for isobutylamine.

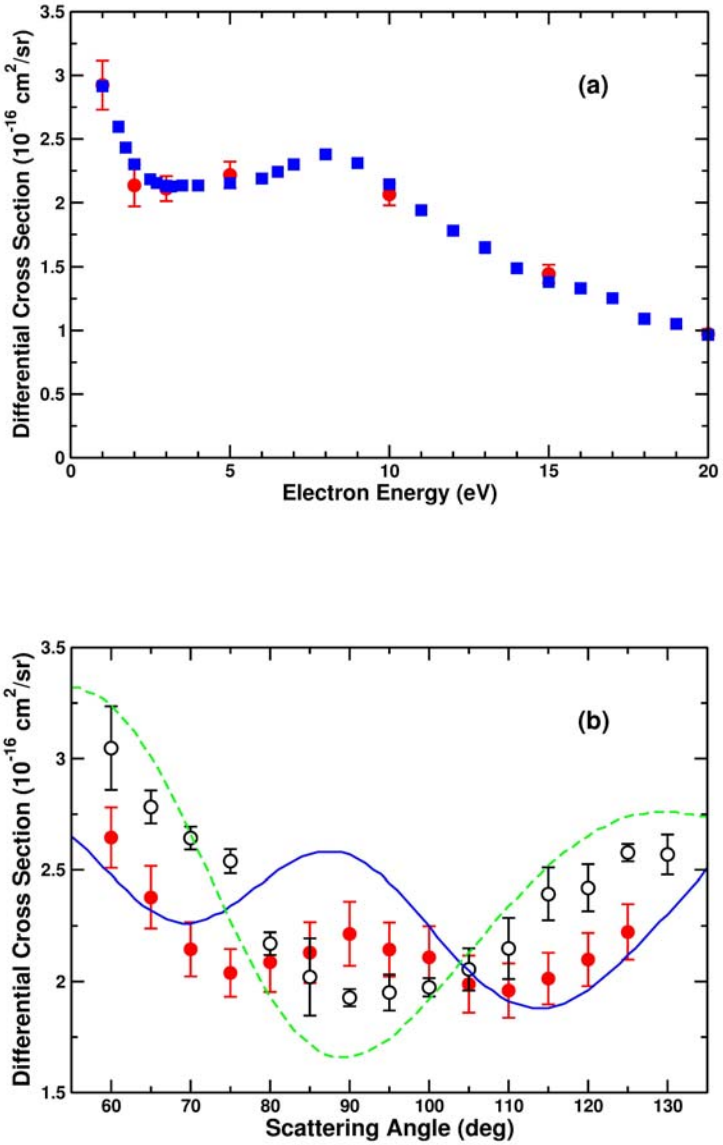

Figure 4 (color online)**.** (a) DCS of isobutanol at θ=90^o as a function of E_0. (b) Detailed view of measured and calculated DCSs for isobutanol and *n*-butanol DCSs at E_0=10eV. Legend is same as for Fig. 3 except solid blue squares in (a) are the excitation function at θ=90^o. See text for discussion.

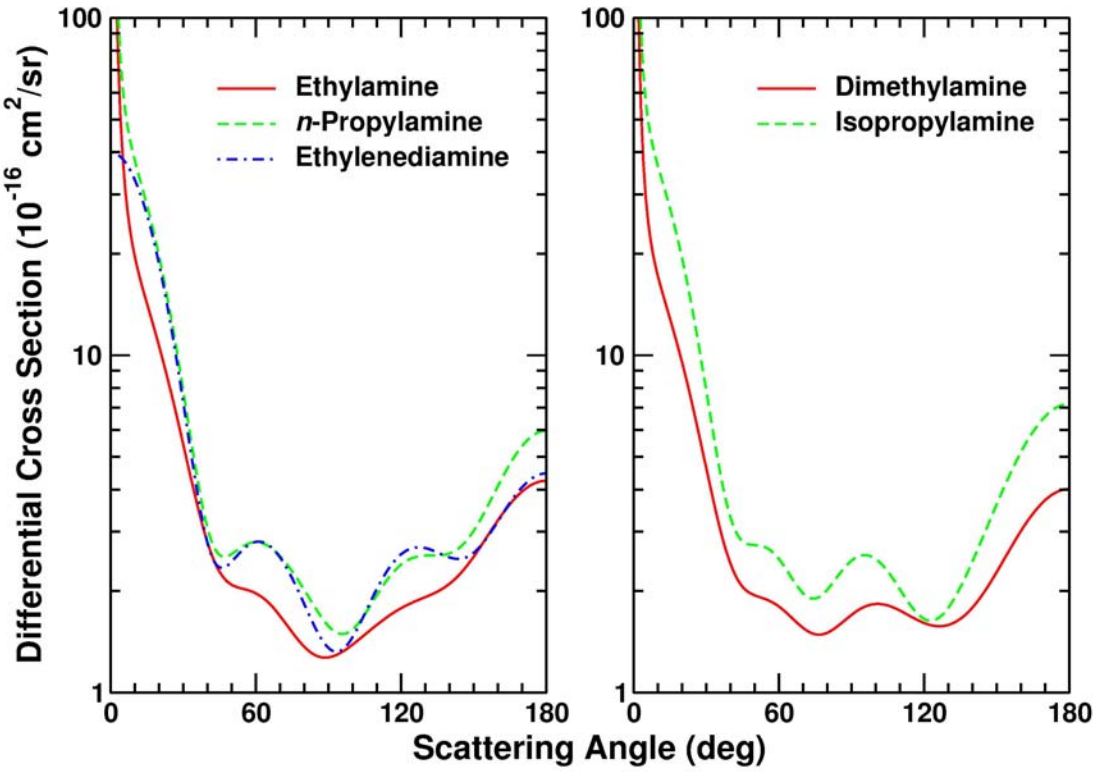

Figure 5 (color online). Calculated differential cross sections at 10 eV impact energy for elastic electron scattering by five small alkyl amines. The molecules in the left panel show primarily an *f*-wave pattern, with a minimum at 90° flanked by two local maxima or shoulders; the molecules in the right panel show an approximate *d*-wave pattern, with a local maximum near 90°.

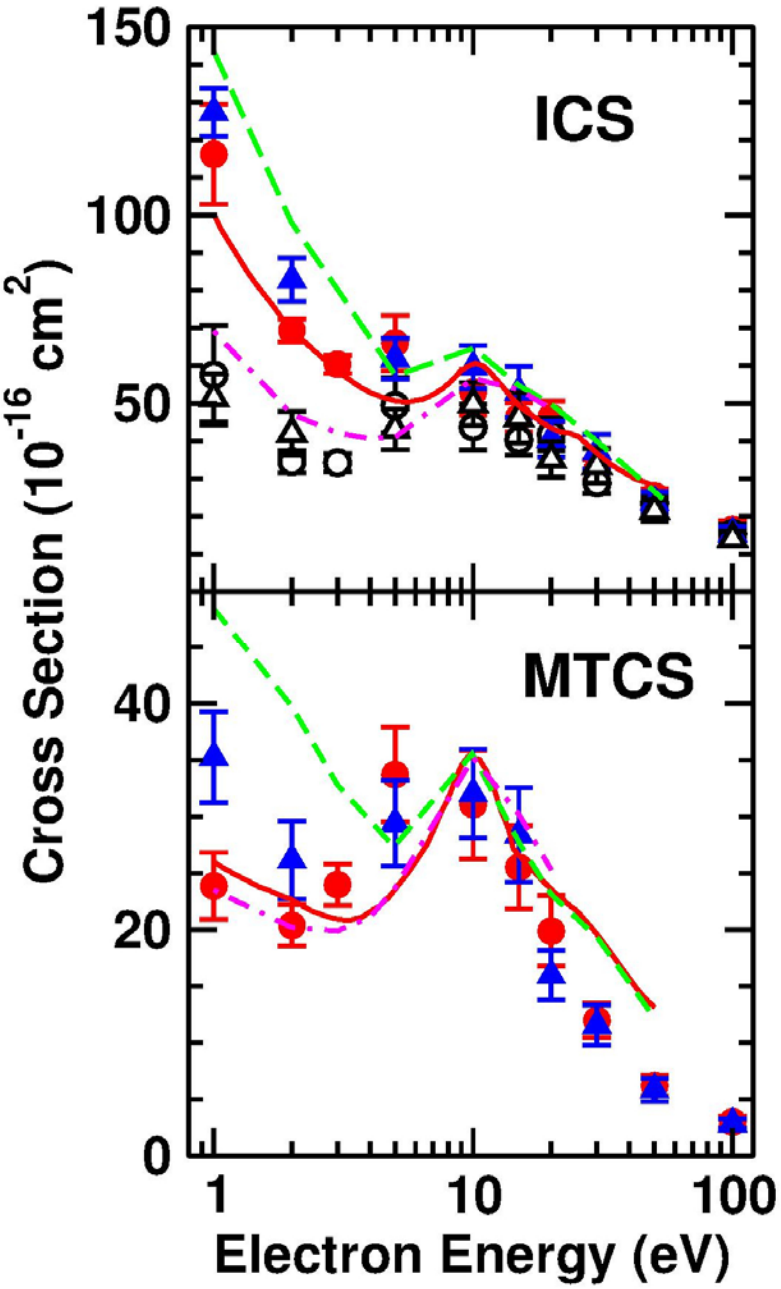

Figure 6 (color online). Integral (top) and momentum transfer (bottom) cross sections for elastic electron scattering by isobutanol and *n*-butanol. The red circles are results for isobutanol obtained using the Born-dipole extrapolation of the present differential cross sections; the blue triangles are results for *n*-butanol obtained in the same way from the differential cross sections of Ref. [3]. The open circles and triangles are corresponding results obtained using a simple polynomial extrapolation. The solid red lines are calculated results for isobutanol from Ref. [4], the dashed green lines are calculated results for *n*-butanol from Ref. [3], and the chained magenta lines are present calculated results for isobutylamine. See text for discussion.